

Resonant behavior and unpredictability in forced chaotic scattering

Alexandre R. Nieto,^{1,*} Jesús M. Seoane,¹ J. E. Alvarillos,² and Miguel A. F. Sanjuán^{1,3}

¹*Nonlinear Dynamics, Chaos and Complex Systems Group,
Departamento de Física, Universidad Rey Juan Carlos,
Tulipán s/n, 28933 Móstoles, Madrid, Spain*

²*Departamento de Física Fundamental, Facultad de Ciencias,
Universidad Nacional de Educación a Distancia,
Paseo Senda del Rey 9, 28040, Madrid, Spain*

³*Institute for Physical Science and Technology,
University of Maryland, College Park, Maryland 20742, USA*

(Dated: June 21, 2018)

Abstract

Chaotic scattering in open Hamiltonian systems is a topic of fundamental interest in physics, which has been mainly studied in the purely conservative case. However, the effect of weak perturbations in this kind of systems has been an important focus of interest in the last decade. In a previous work, the authors studied the effects of a periodic forcing in the decay law of the survival probability, and they characterized the global properties of escape dynamics. In the present paper, we add two important issues in the effects of periodic forcing: the fractal dimension of the set of singularities in the scattering function, and the unpredictability of the exit basins, which is estimated by using the concept of basin entropy. Both the fractal dimension and the basin entropy exhibit a resonant-like decrease as the forcing frequency increases. We provide a theoretical reasoning, which could justify this decreasing in the fractality near the main resonant frequency, that appears for $\omega \approx 1$. We attribute the decrease in the basin entropy to the reduction of the area occupied by the KAM islands and the basin boundaries when the frequency is close to the resonance. Finally, the decay rate of the exponential decay law shows a minimum value of the amplitude, A_c , which reflects the complete destruction of the KAM islands in the resonance. We expect that this work could be potentially useful in research fields related to chaotic Hamiltonian pumps, oscillations in chemical reactions and companion galaxies, among others.

PACS numbers: 05.45.Ac,05.45.Df,05.45.Pq

*alexandre.rodriquez@urjc.es

I. INTRODUCTION

Chaotic scattering in open Hamiltonian systems has been an interesting topic of research in nonlinear dynamics and chaos theory due to its numerous applications in several fields of physics, such as celestial mechanics, fluid mechanics and atomic and nuclear physics (see Ref. [1] for an exhaustive description of the applications of chaotic scattering).

In a generic situation of chaotic scattering, the particles enter a finite region where they experience some sort of transient chaotic dynamics due to the interaction with a potential, and then leave the region. In this sense, the phenomenon could be understood as a manifestation of transient chaos [2, 3]. Far enough from the scattering region, the action of the potential is negligible so the particle motion is essentially free. A usual tool in chaotic scattering is the scattering function, which represents the relation between characteristic variables of the input and the output of the scattering region. When the scattering is nonchaotic, the scattering function will be formed by smooth curves, which leads to a high capacity to predict the behavior of one of the variables from the other. In chaotic scattering problems, the scattering function has a set of singularities as a result of the sensitive dependence to the initial conditions, which constitutes a hallmark of chaos. If we go into the neighborhood of one of the singularities, we will conclude that the range of variation of the output variable does not tend to zero as the size of the neighborhood is arbitrarily reduced.

Chaotic scattering processes have been studied in several physical systems such as hard-disk systems [4] and billiard systems [5, 6], although much of the literature refers to open Hamiltonian systems (e.g. [7–10]), where the Hénon-Heiles Hamiltonian constitutes a well-known paradigm (e.g. [11–15]). The Hamiltonian is given by

$$\mathcal{H} = \frac{1}{2}(\dot{x}^2 + \dot{y}^2) + \frac{1}{2}(x^2 + y^2) + x^2y - \frac{1}{3}y^3. \quad (1)$$

This system is conservative and hence the energy is conserved. Furthermore, it has a critical value of the energy $E_e = 1/6$ such that for lower values, i.e., $E \leq E_e = 1/6$, the isopotential curves are closed. For larger values $E > E_e = 1/6$ the isopotential curves are open and the particles can escape from the scattering region and go to infinity through three different *exits* (See Fig. 1(b)).

Much work has been done in the past decade concerning the effect of different perturbations such as noise, dissipation and periodic forcing [16–22] in the escape dynamics of this system under the assumptions of Newtonian dynamics. Recently, the Hénon-Heiles Hamiltonian has been

also studied in the relativistic case [23, 24]. The evolution of the fractal dimension of the scattering function has been studied in the presence of dissipation, noise and relativistic corrections; but not in the presence of forcing. This is one of the main motivations for which we have decided to analyze the periodically forced Hénon-Heiles system.

Because of the chaotic dynamics, particles with slightly different initial conditions can describe completely different trajectories and escape through different exits. Therefore, chaotic scattering implies some sort of unpredictability, understanding it as the difficulty of predicting the exit through which a trajectory will escape. In a Hamiltonian system, since the total energy is conserved, we cannot speak about attractors, and thus, we cannot define basins of attraction [25, 26]. However, in an open Hamiltonian system, we can define exit basins [27] in an analogous way to the basins of attraction in dissipative systems. We say that the exit basin associated with the exit i is the set of initial conditions whose trajectories will escape through the exit i . In the case of the Hénon-Heiles system, there exist three exit basins and, in the nonhyperbolic regime, a set of initial conditions for the particles that will never escape from the scattering region. To quantify the unpredictability of the escape basins, we use the basin entropy as a useful tool to analyze the exit basins associated with a large set of parameters (in our particular case the forcing amplitude and frequency), which is another issue we add in this paper.

This paper is organized as follows. In Sec. II, we describe our model, the periodically forced Hénon-Heiles system. The effects of forcing in the fractal dimension of the scattering function are carried out in Sec. III. In that section we also provide a theoretical reasoning that could justify the obtained results. The qualitative effects of the forcing term on the basin topology are shown in Sec. IV. In Sec. V, we evaluate the unpredictability of the exit basins using the concept of basin entropy. Finally, in Sec. VI, we present the main conclusions of this manuscript.

II. MODEL DESCRIPTION

The Hénon-Heiles system appeared in literature for the first time in 1964 in an article by the astronomers Michel Hénon and Carl Heiles [28]. Both researchers worked in the search for a third

integral of motion in galactic systems. The equations of motion are given by

$$\begin{aligned}
\dot{x} &= p, \\
\dot{p} &= -x - 2xy \\
\dot{y} &= q, \\
\dot{q} &= -y - x^2 + y^2,
\end{aligned} \tag{2}$$

where p and q denote the two components of the generalized momentum.

We focus our attention in the effects of the periodic forcing on the chaotic scattering. In this context, the periodic forcing is introduced in a natural way as follows [29]:

$$\begin{aligned}
\dot{p} &= -x - 2xy + A_x \sin \omega_x t, \\
\dot{q} &= -y - x^2 + y^2 + A_y \sin \omega_y t,
\end{aligned} \tag{3}$$

where we take, for simplicity and without loss of generality, the same amplitudes ($A_x = A_y = A$) and frequencies ($\omega_x = \omega_y = \omega$). One of the physical motivations to introduce the forcing in this kind of systems is the study of spiral galaxies in Astronomy and Astrophysics in which the forcing is a natural ingredient as shown in Ref. [30].

To intuitively visualize the system, we plot the potential and the isopotential curves for different values of the energy in Fig. 1.

For energies $E > E_e$ the trajectories may come from infinity or from inside the scattering region, and after interacting with the potential, they escape through one of the exits. One of the properties of the Hénon-Heiles system is the existence of three highly unstable periodic orbits known as Lyapunov orbits [31], each one located in the vicinity of one of the exits. When a trajectory passes through a Lyapunov orbit with its velocity vector pointing outwards of the scattering region, it will escape to infinity and will never come back.

The addition of a periodic forcing term can change the dynamics of the system in a drastic way [17]. In Fig. 2, we show four trajectories in the presence of forcing of amplitude $A = 0.01$ with different frequencies. Figures 2(a)-(c) show three trajectories escaping through different exits after passing through the scattering region. In Fig. 2(d) we show a quasiperiodic orbit. All the trajectories have been launched from the same initial point $(x_0, y_0) = (0.0, 0.65)$ with the same energy $E = 0.19$. In this figure we can see how the frequency of a forcing term with a small amplitude can modify the exit through which the particle escapes.

Even for values $E > E_e$ there exist initial conditions that generate trajectories that will remain

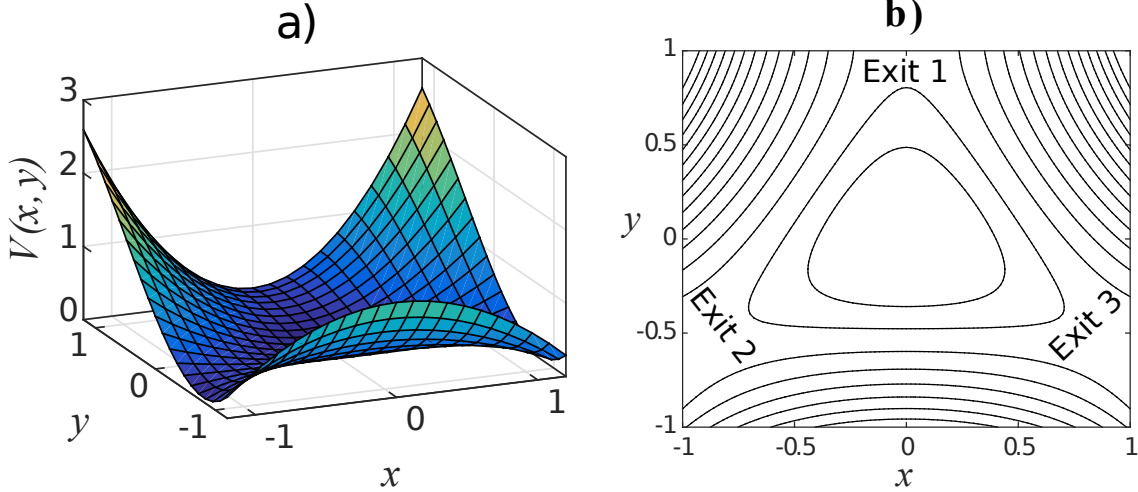


FIG. 1: (Color online) (a) Potential energy $V(x, y)$ associated to the the Hénon-Heiles system. (b) The isopotential curves for different values of the energy $E \in [0.08, 1.5]$. The curves are closed for energies below the threshold value $E_e = 1/6$, and they exhibit three symmetrical exits, separated by an angle of $2\pi/3$ radians, when the energy $E > E_e$.

forever within the scattering region. These trajectories are typically quasiperiodic. Quasiperiodic orbits are trajectories that periodically return to a finite region of the phase space but never close on themselves, which belong to a Kolmogorov-Arnold-Moser (KAM)-island [32]. The existence of these islands is one of the main characteristics of nonhyperbolic chaotic scattering and as a consequence the decay law of the survival probability is algebraic. When the scattering is hyperbolic, the stable and unstable manifolds of the chaotic saddle are never tangent and every saddle point is hyperbolic [33]. In addition there are no KAM islands mixed with the chaotic saddle and consequently the decay law becomes exponential. We are particularly interested among other things in the dynamics of the system associated with KAM islands. This justifies that we have considered the nonhyperbolic regime, which is manifested for energies in the approximate range $E \in [E_e, 0.23]$ [17], while the hyperbolic regime is associated to values of $E \gtrsim 0.23$.

III. FRACTAL DIMENSION

The scattering function presents fractal geometry, which implies some sort of unpredictability when relating the input and output variables in the scattering region. We can quantify this unpredictability through the computation of the fractal dimension of the set of singularities of the

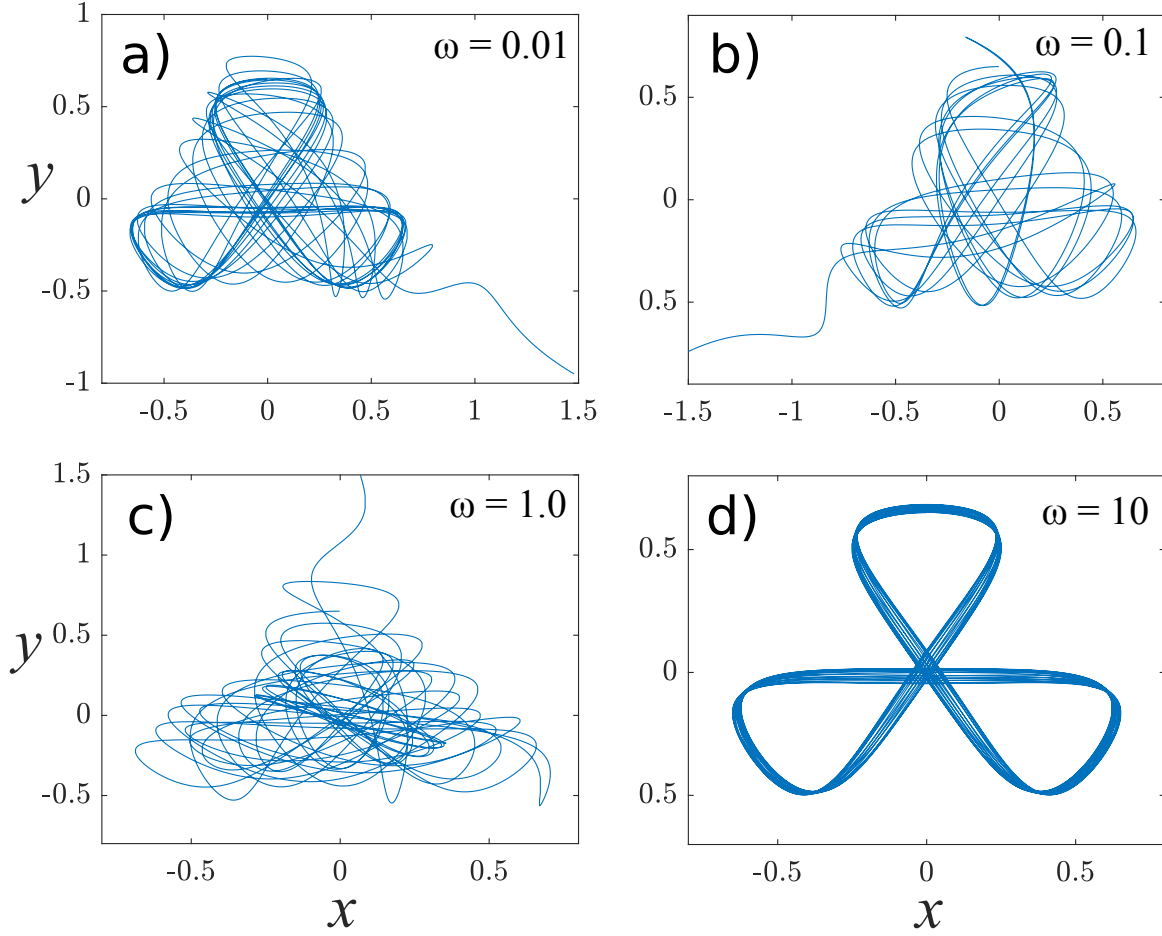


FIG. 2: (Color online) Trajectories in the forced Hénon-Heiles system with energy $E = 0.19$ and $A = 0.01$. Panels (a)-(c) show three trajectories escaping through different exits due to the effects of the periodic forcing term of frequencies $\omega = 0.01$, $\omega = 0.1$ and $\omega = 1.0$, respectively. Panel (d) shows a quasiperiodic orbit for the frequency $\omega = 10.0$. In all the trajectories the initial condition is $(x_0, y_0) = (0.0, 0.65)$. This initial condition is associated with a KAM island in the conservative case. We can clearly observe the role of the frequency, which can change drastically the destination of the particle.

scattering function. Previous researchers [34] conjectured, providing numerical evidence, that in nonhyperbolic chaotic scattering the set of singularities of the scattering function has Lebesgue measure zero and its fractal dimension is always $D = 1$. This value implies that the difficulty to determine the output variable from the input variable is maximal. The value $D = 1$ is justified based on the algebraic decay law of the survival probability.

To perform the calculation of the fractal dimension, we use the uncertainty algorithm given in [35, 36]. In particular, we launch the trajectories from the line segment defined by the points

$(x, y) = (0, -0.5)$ and $(x, y) = (0, 0)$. In order to fix the value of \dot{y} we use the tangential shooting method [11], in which the trajectories are launched towards the scattering region in such a way that the velocity vector is tangent to a circumference centered at the origin and passing through the point (x_0, y_0) . For a given initial condition y_0 we choose another initial condition $y_0 + \delta$, where δ is some small perturbation. For a fixed value of the uncertainty δ , we compute the escape time (T) of both trajectories, and we say that the initial condition is uncertain if $|T(y_0) - T(y_0 + \delta)| > h$, where h is the integration step of the numerical method (a fourth-order Runge-Kutta method in our case).

The fraction of uncertain initial conditions obeys the law [34]:

$$f(\delta) \sim \delta^{1-D}. \quad (4)$$

Taking logarithms in the above equation we obtain

$$\log \frac{f(\delta)}{\delta} = -D \log \delta + k, \quad (5)$$

where k is a constant. This equation allows us to obtain the fractal dimension D computationally from the slope of the line that must yield a representation $\log(f(\delta)/\delta)$ versus $\log \delta$.

In all the simulations of this section we have set $h = 0.005$ and we have taken 21 values of δ from 10^{-9} to 10^{-5} . In Fig. 3 we represent the results for both the conservative case and forced case with amplitude $A = 0.05$ and a frequency $\omega = 1$. In this case, in order to obtain the fraction of uncertain initial conditions, we have taken 50000 initial conditions for each δ . In both cases we observe a strict linear relation between the variables. The fractal dimension is estimated to be $D = 0.99$ in the conservative case and $D = 0.72$ in the forced case.

First, we want to clarify the effect of the frequency and the amplitude on the fractal dimension. We have obtained the fractal dimension for 250×250 values of $A \in [0, 0.05]$ and $\omega \in [0, 5]$ for $E = 0.17$. In each case the fraction of uncertain initial conditions was obtained by throwing 50000 initial conditions selected by sweeping along the segment defined by the points $(x, y) = (0, -0.5)$ and $(x, y) = (0, 0)$. A good way to represent these results is using a color-code map in the (ω, A) plane. The results are shown in Fig. 4. The hot colors indicate larger values of the fractal dimension. In the figure we observe a resonant-like behavior where the critical values for the frequency are $\omega \approx 1$ and $\omega \approx 2$. For values close to $\omega = 1$ the fractal dimension drastically decreases and does it again, less abruptly, when $\omega \approx 2$. When the second resonant frequency is exceeded, the fractal dimension returns monotonously to $D \approx 1$. The decrease occurs for the same

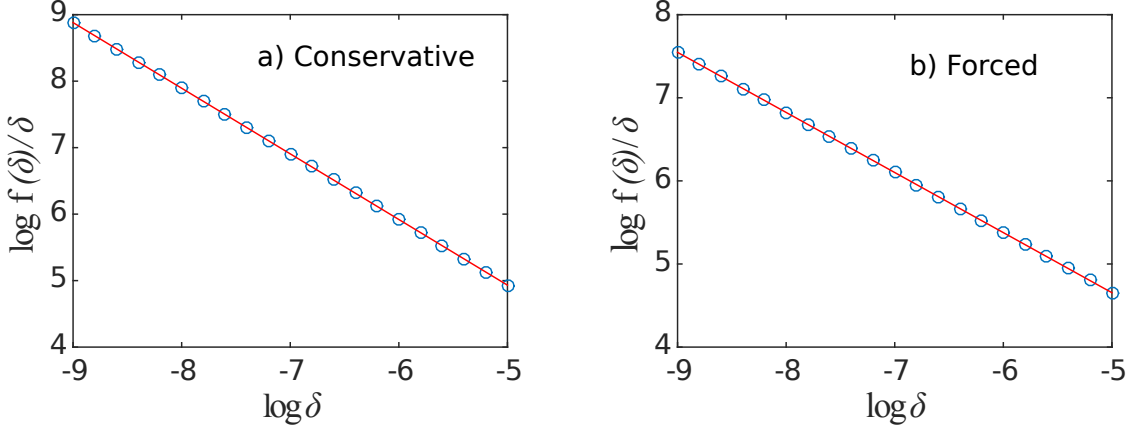


FIG. 3: (Color online) Algebraic scaling between $f(\delta)/\delta$ and δ for $E = 0.17$. (a) For the conservative case. (b) Forced case with amplitude $A = 0.05$ and frequency $\omega = 1$. The fractal dimension is estimated to be $D = 0.99$ in the conservative case and $D = 0.72$ in the forced case.

value of ω regardless of the amplitude, although the decrease will be greater for higher amplitude values.

In order to generalize the previous results for any energy within the nonhyperbolic regime, we have set $A = 0.05$ and computed the fractal dimension for different values of the frequency and the energy. Specifically, we have taken 250×250 combinations of energy $E \in [0.17, 0.20]$ and frequency $\omega \in [0, 5]$. We have again constructed a color-code map, which is represented in Fig. 5. From this figure it follows that the evolution of the fractal dimension with the forcing frequency is qualitatively the same within the nonhyperbolic regime. In the same way as in Fig. 4, the minimum of the fractal dimension associated with the resonant frequencies can be clearly observed.

Now we provide a theoretical reasoning that could justify the effects of the forcing near the resonance, using the fractal dimension of Cantor-like structures as a parallelism. In systems where chaotic scattering occurs, particles are launched from a line segment straddling the stable manifold of the chaotic saddle. There is a certain interval of the input variable which lead to trajectories that remain in the scattering region for at least a time T_0 . By a time $2T_0$ a fraction η of the remaining particles leave the scatterer. If these particles are located in the middle of the original interval, we are left with two equal-length subintervals of the input variable that lead to trajectories that do not escape for, at least, a duration of time $2T_0$. By a time $3T_0$ an additional fraction η of the

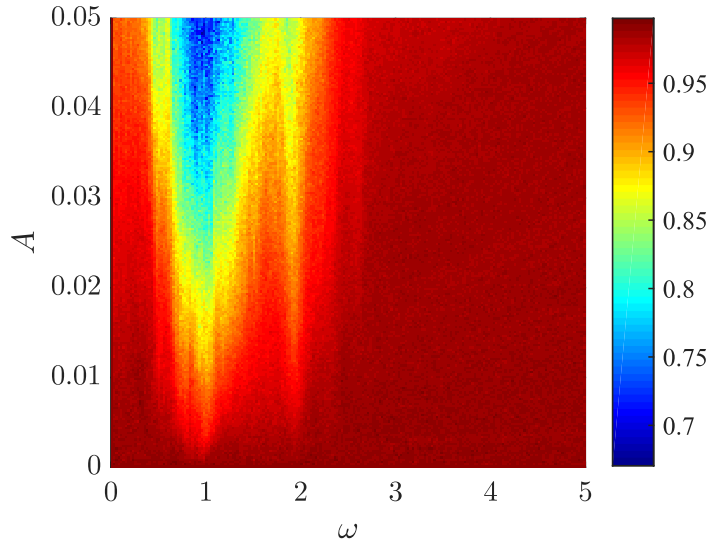


FIG. 4: (Color online) Color-code map of the fractal dimension for several values of the forcing frequency and amplitude in the periodically forced Hénon-Heiles system with $E = 0.17$. We have used 250×250 equally spaced values of the parameters. The hot colors indicate larger values of the fractal dimension. It can be observed that, for any non-zero amplitude, the fractal dimension exhibits a resonant-like evolution, where $\omega \approx 1$ and $\omega \approx 2$ are the main frequencies.

particles remaining at time $2T_0$ leave the scatterer. We assume that these particles were located in the middle of the first two subintervals. If we continue this iterative proceeding we obtain a Cantor-like set of Lebesgue measure zero with associated fractal dimension, D , given by

$$D = \frac{\ln 2}{\ln [2/(1 - \eta)]}. \quad (6)$$

On the other hand, for high amplitudes, near the resonant frequency, say $\omega \in [0.8, 1.2]$, KAM islands are destroyed and then the decay law becomes exponential. In this case the decay rate is related to the fraction η remaining at each stage of the construction of the Cantor-like set by

$$\gamma(\omega) = \frac{1}{T_0} \ln (1 - \eta)^{-1}. \quad (7)$$

According to Eqs. (6) and (7) we find a relation between the fractal dimension and the decay rate

$$D = \frac{\ln 2}{\ln 2 + T_0 \gamma(\omega)}. \quad (8)$$

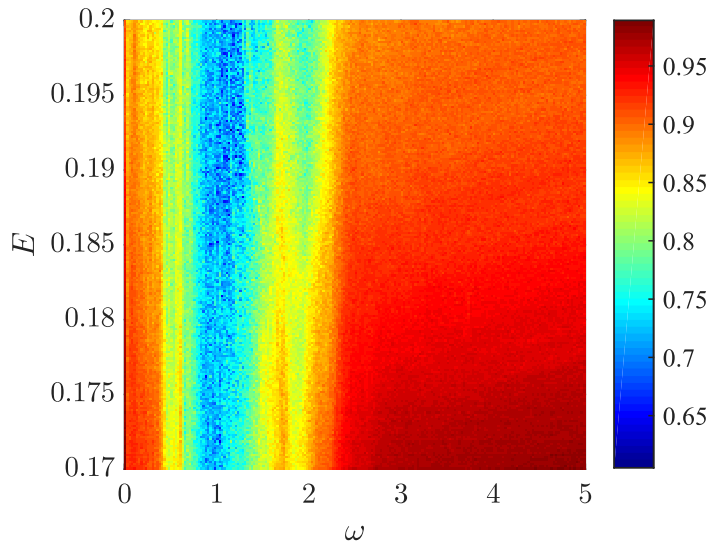


FIG. 5: (Color online) Color-code map of the fractal dimension for several values of the forcing frequency and energy in the periodically forced Hénon-Heiles system with $A = 0.05$. We have used 250×250 equally spaced values of the parameters. The hot colors indicate larger values of the fractal dimension. It can be observed that, for any energy within the nonhyperbolic regime, the fractal dimension exhibits a resonant-like evolution, where $\omega \approx 1$ and $\omega \approx 2$ are the main frequencies.

If we increase ω , approaching the resonant frequency, the amount of particles remaining at each time is reduced and then we expect $d\gamma/d\omega > 0$. On the other hand, once the resonant frequency is reached, if we increase ω we expect $d\gamma/d\omega < 0$. According to Eq. 8, since $\gamma(\omega) > 0$, $d\gamma/d\omega > 0$ implies $dD/d\omega < 0$. In the same way $d\gamma/d\omega < 0$ leads to $dD/d\omega > 0$. These theoretical reasoning is in good agreement with the numerical results showed in Fig. 4 and Fig. 5. In order to observe clearly the change in sign of $dD/d\omega$ in Fig. 6, we plot the computed fractal dimension of the scattering function versus the forcing frequency for $E = 0.17$ and different values of the amplitude. To perform the dimension calculation we launched, for each frequency, 50000 initial conditions $\theta_0 \in [0, 2\pi]$ from the point $(x_0, y_0) = (0.15, -0.25)$. In this figure, we clearly observe the decrease of the fractal dimension near the frequencies $\omega \approx 1$ and $\omega \approx 2$. The resonant-like behavior occurs for the three amplitudes considered, being the decrease of the fractal dimension greater for larger amplitudes.

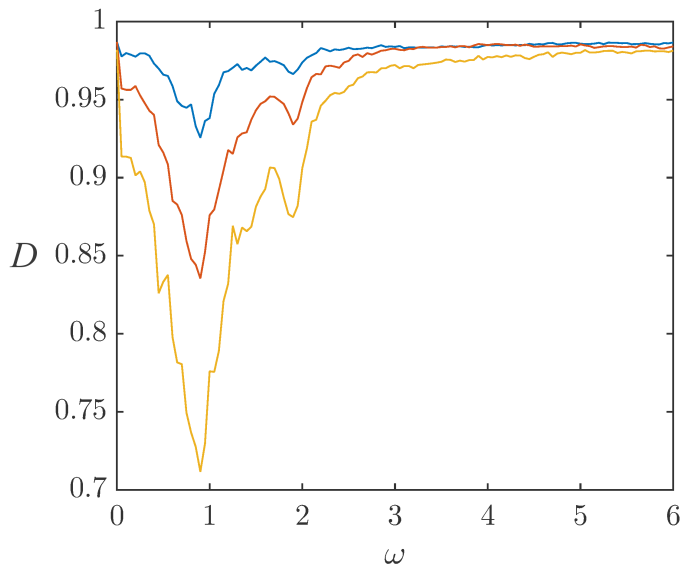


FIG. 6: (Color online) Fractal dimension of the scattering function for $E = 0.17$ and different values of amplitude $A = 0.01$ (blue), $A = 0.03$ (red) and $A = 0.05$ (yellow). For each frequency, to calculate the fraction of uncertain initial conditions, 50000 initial conditions $\theta_0 \in [0, 2\pi]$ have been launched from the point $(x_0, y_0) = (0.15, -0.25)$.

IV. BASIN TOPOLOGY

To obtain the exit basins, we choose a uniform grid of 500×500 initial conditions in the plotted region. We plot each initial condition with a different color depending on the exit through which the trajectory escapes. We have selected the initial conditions in the physical space (x, y) using the tangential shooting method. In Fig. 7 we represent two exit basins in the conservative case with different values of the energy. In the basin obtained for $E = 0.17$ we can observe well-defined regions where the particles will never escape (nonhyperbolic regime), but the same does not occur for $E = 0.25$ (hyperbolic regime).

The destruction of the KAM islands can be observed intuitively in the exit basins. For two different energies in the nonhyperbolic regime ($E = 0.17$ and $E = 0.19$) we have obtained the exit basins with resolution 500×500 for a forcing amplitude $A = 0.05$ and 51 frequencies in the range $\omega \in [0, 5]$. The only frequencies that lead to the destruction of the KAM islands are $\omega = 0.9$ and $\omega = 1.0$. In Fig. 8 we plot the exit basins for $\omega = 0.0$ and $\omega = 1.0$.

A natural question at this point is: what is the critical value of the forcing amplitude, A_c , that

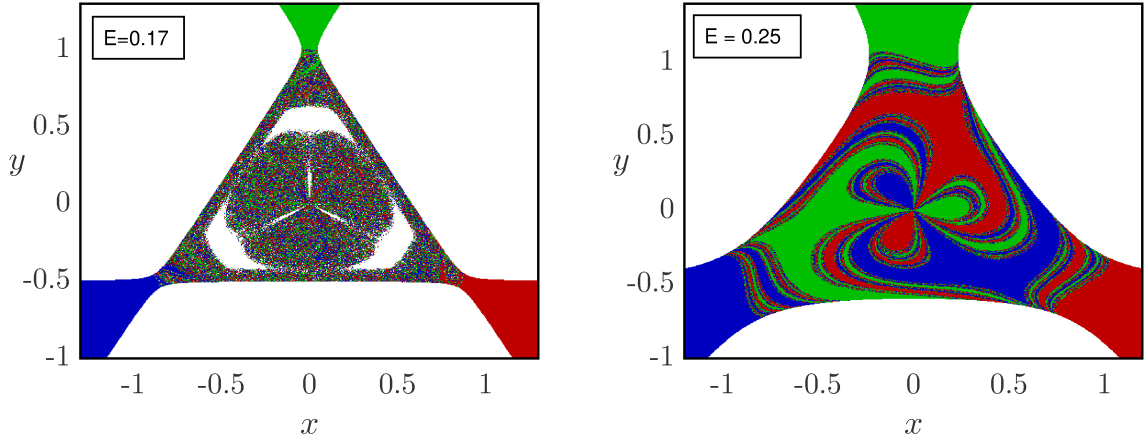


FIG. 7: (Color online) Exit basins in the physical space (x, y) for the conservative Hénon-Heiles system for the energy values indicated in each figure. The color code is as follows: green, blue and red correspond to the initial conditions that lead to exits 1, 2 and 3, respectively, and white corresponds to bounded orbits that never escape.

allows the destruction of the KAM islands in the resonance? We have obtained its value for 14 values of the energy in the range $E \in [0.17, 0.2]$ for $\omega = 0.9$. The value obtained is $A_c = 0.015$ in all cases.

In nonhyperbolic chaotic scattering the particle decay law is algebraic and there exist KAM islands mixed with the chaotic saddle in the phase space. But if the amplitude is large enough, a forcing close to the resonance frequency $\omega = 1$ destroys the KAM islands. Therefore all the particles will escape in a finite time and the decay law becomes exponential

$$R(t) \sim e^{-\gamma t}, \quad (9)$$

where $R(t)$ is the fraction of particles that survive at time t and $\gamma \geq 0$ is the decay rate.

For values $\omega \approx 1$ the decay rate is approximately constant within the nonhyperbolic regime. For 31 values of the energy in the range $E \in [0.17, 0.2]$ we have obtained (with $A = 0.05$) $\gamma = (3.318 \pm 0.033) \times 10^{-2}$ for $\omega = 1.0$ and $\gamma = (5.648 \pm 0.097) \times 10^{-2}$ for $\omega = 0.9$. We have considered an error $\varepsilon_\gamma = 3\sigma(\gamma)/\sqrt{n}$, where $n = 31$ is the number of samples and σ is the standard deviation. To obtain the decay rate we have used 10^6 initial conditions, using an equally spaced 1000×1000 grid in the physical space (x, y) . For each initial condition we compute the escape time and determine the fraction that remains in steps $\Delta t = 20$. Finally, we represent $\ln R$ versus t and we obtain the decay rate from the slope of the straight line. For example, Fig. 9 shows the

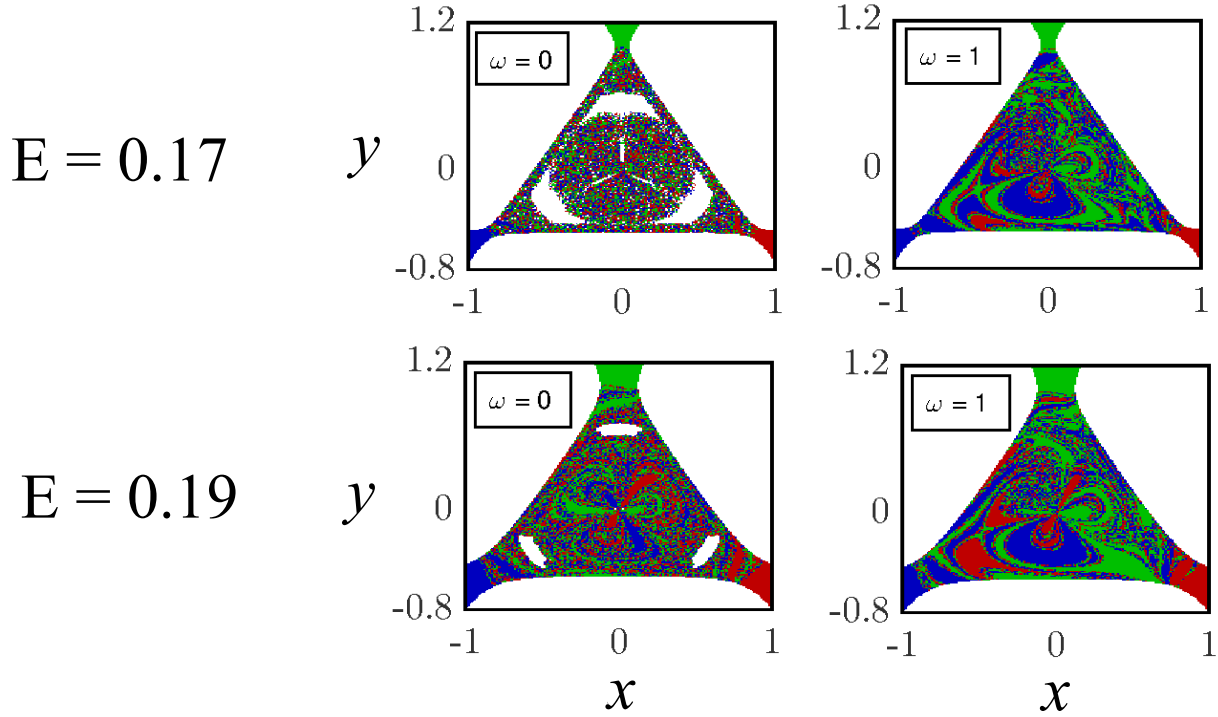


FIG. 8: (Color online) Exit basins in the physical space (x, y) for the forced Hénon-Heiles system when the forcing amplitude is $A = 0.05$. The energy value is $E = 0.17$ (upper) and $E = 0.19$ (lower) and the frequency value is indicated in each figure. The color code is as described in the caption to Fig. 7.

straight line obtained by the least squares method for $E = 0.19$ with a frequency forcing $\omega = 0.9$ and amplitude $A = 0.05$.

Another consequence of a forcing with a frequency close to resonance is the decrease in the area occupied by the basin boundaries. Given an energy $E = 0.19$ and a forcing frequency $\omega = 0.9$, the fraction of the area of the basins occupied by the boundaries decreases with increasing amplitude, as shown in Fig. 10, where we plot the boundaries of the basins for different values of the amplitude. The fraction occupied by the boundaries is: 0.82 ($A = 0$), 0.71 ($A = 0.01$), 0.45 ($A = 0.05$) and 0.23 ($A = 0.1$).

V. BASIN ENTROPY

Sometimes in nonlinear dynamics, unpredictability is defined as the difficulty to predict the evolution of the orbits [37–39]. In the context of open Hamiltonian systems, we consider unpre-

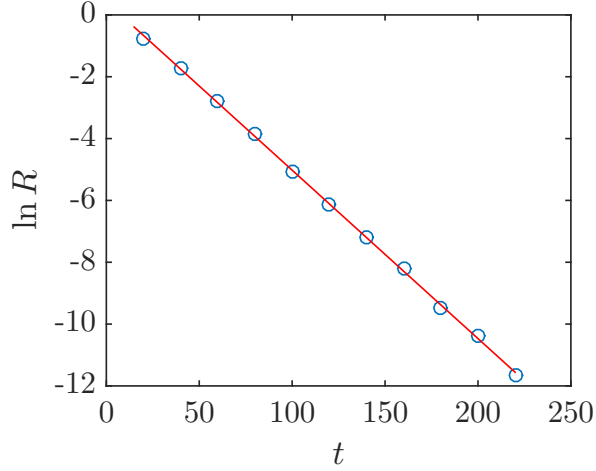


FIG. 9: (Color online) Exponential decay law for the particles remaining in the scattering region at time t . R denotes the fraction of particles that survive in a time t . The energy is $E = 0.19$ and the forcing amplitude and frequency are $A = 0.05$ and $\omega = 0.9$. The decay rate is estimated to be $\gamma = 5.45 \times 10^{-2}$.

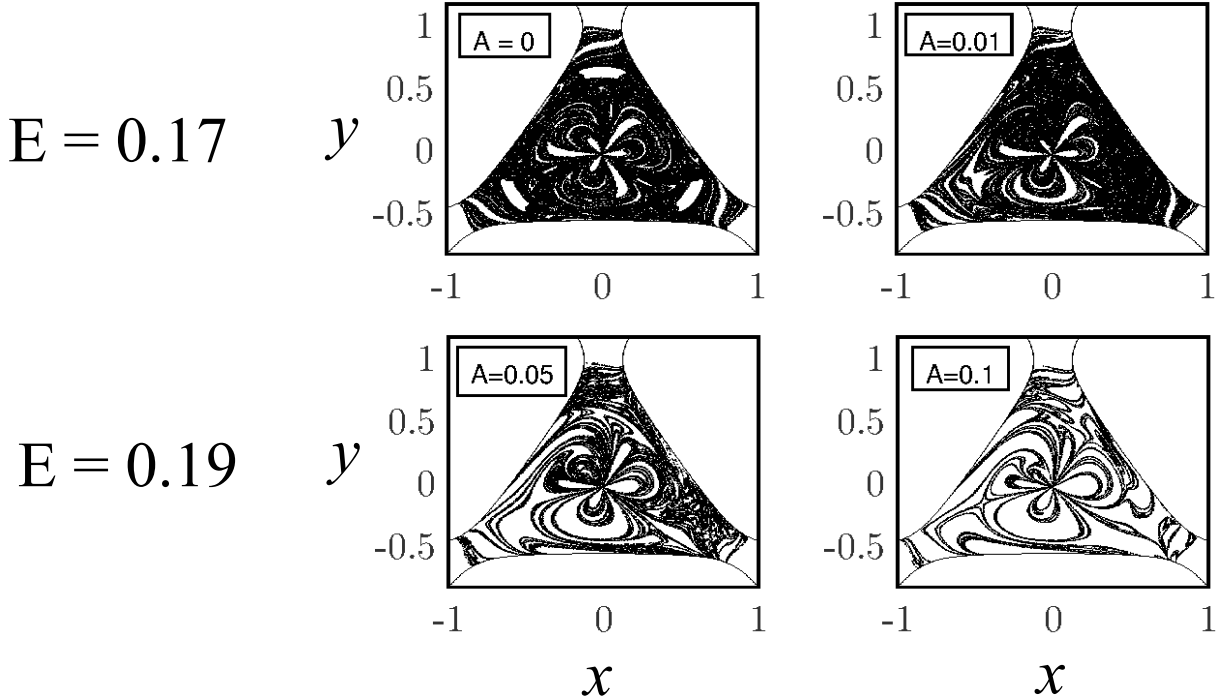


FIG. 10: Boundaries of the exit basins in the physical space (x, y) when the energy is $E = 0.19$ and the forcing frequency $\omega = 0.9$. The value of the amplitude is indicated in each figure. The fraction occupied by the boundaries is: 0.82 ($A = 0$), 0.71 ($A = 0.01$), 0.45 ($A = 0.05$) and 0.23 ($A = 0.1$).

dictability as the difficulty in determining the final state of a system from certain initial conditions. In this sense, the topology of the exit basins in open Hamiltonian systems, or the topology of the basins of attraction in dissipative systems, is closely related to the unpredictability of the system. One probably say that in Fig. 7 the basin for $E = 0.17$ is more unpredictable than the basin for $E = 0.25$. The basin entropy [40] is a tool that allows us to quantify the unpredictability that we detect intuitively in the basins. It also allows to study and quantify the unpredictability for a large set of basins.

The method to compute the basin entropy is as follows. We randomly select N overlapping square boxes of linear size ε and we obtain the entropy of each one of the boxes:

$$S_i = \sum_{j=1}^{m_i} \frac{n_{i,j}}{\varepsilon^2} \ln \left(\frac{\varepsilon^2}{n_{i,j}} \right), \quad (10)$$

where m_i is the number of different destinations (*colors*) in the box i and $n_{i,j}$ is the number of points with color j in the box. In the Hénon-Heiles system $m_i \in [1, 3]$ in the hyperbolic regime and $m_i \in [1, 4]$ in the nonhyperbolic regimen, due to the existence of quasiperiodic orbits.

The entropy associated to all the N boxes is:

$$S = \sum_{i=1}^N \sum_{j=1}^{m_i} \frac{n_{i,j}}{\varepsilon^2} \ln \left(\frac{\varepsilon^2}{n_{i,j}} \right). \quad (11)$$

Finally, we obtain the basin entropy by scaling the total entropy S to the total number of boxes, $S_b = S/N$. After this scaling the basin entropy is normalized between 0 and $\ln N_d$, where N_d is the number of different destinations. The value 0 is associated with a basin that has a unique destination and the value $\ln N_d$ is associated with a basin with equiprobable and randomly distributed destinations.

In all the simulations of this section we work in the region $\Omega \in [-1, 1] \times [-0.8, 1.2]$ of the physical space (x, y) , using exit basins of resolution 500×500 . The value of the basin entropy depends on the linear box size ε . Therefore we have to select an adequate value of ε that allows a reliable portrait of the unpredictability of the basins. We have chosen $\varepsilon = 0.02$, that is, 25 trajectories in each box. We consider that this value accounts for the internal structure of the basins and allows a statistically significant approximation of the probabilities of each color in the box.

We have mentioned that some of the effects of a forcing close to the resonant frequency are the destruction of the KAM islands and the decrease in the area occupied by the boundaries of the exit basins. The basin entropy gives an account, among other things, for these two important changes

in the topology and allows a reliable portrait of the evolution of unpredictability according to the forcing frequency and amplitude. For $E = 0.19$ we have computed 100×100 basins for different combinations of amplitude $A \in [0, 0.05]$ and frequency $\omega \in [0, 5]$. For each of these 10000 basins we have obtained the basin entropy, shown in the color-code map of Fig. 11.

From the color-code map we conclude that there is a resonant-like behavior for the evolution of the unpredictability of the exit basins. The main resonant frequency is $\omega \approx 1$ and it coincides with that obtained in the case of the fractal dimension of the scattering function in Sec. III.

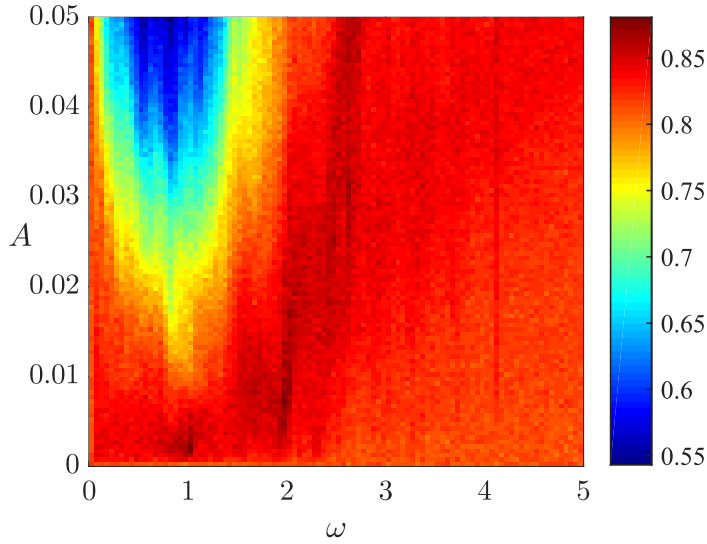


FIG. 11: (Color online) Color-code map of the basin entropy for several values of the forcing frequency and amplitude, with $E = 0.19$. We have used 100×100 values of the parameters. The hot colors indicate larger values of the basin entropy.

The color-code map also shows that the basin entropy exceeds the value of the unperturbed case for a frequency value $\omega \approx 2.5$. To observe this point with greater clarity, in Fig. 12 we represent the basin entropy as a function of the forcing frequency for $E = 0.19$ and $A = 0.05$. In this simulation, 100 exit basins with a resolution 1000×1000 have been computed. In Fig. 12 we can distinguish three different regions: (a) $\omega \in (0, 2.0)$, resonant-like behavior; (b) $\omega \in (2.0, 3.2)$, maximum value of basin entropy and (c) $\omega \in (3.2, 10.0)$, the forcing becomes unproductive. In the region (a) the basin entropy decreases until reaching its minimum value for $\omega \approx 1.0$ and then increases until reaching the value of the undisturbed case. In the region (b) the maximum value of the basin entropy is obtained for $\omega \approx 2.5$. For this frequency value the fractal dimension of the scattering function was not noticeably affected, but the same does not happen with the basin

entropy. This is because this maximum is associated with an increase in the area occupied by the KAM islands. Since in our simulations we have considered that the particles that never escape constitute a destination of the dynamical system, the basin entropy is influenced by both the topology and the area of the KAM islands. The scattering function represents the relation between the escape times of particles and one of the characteristic parameters of the system. Therefore trajectories that never escape are excluded from the scattering function and their fractality is not influenced by the changes in the KAM islands. Finally, in the region (c) the forcing begins to be irrelevant and the basin entropy converges monotonously to the undisturbed case, as shown in the horizontal dashed line. In this last situation, the frequency has no visible effects on the unpredictability of the system when it is large enough, as shown in Ref. [29].

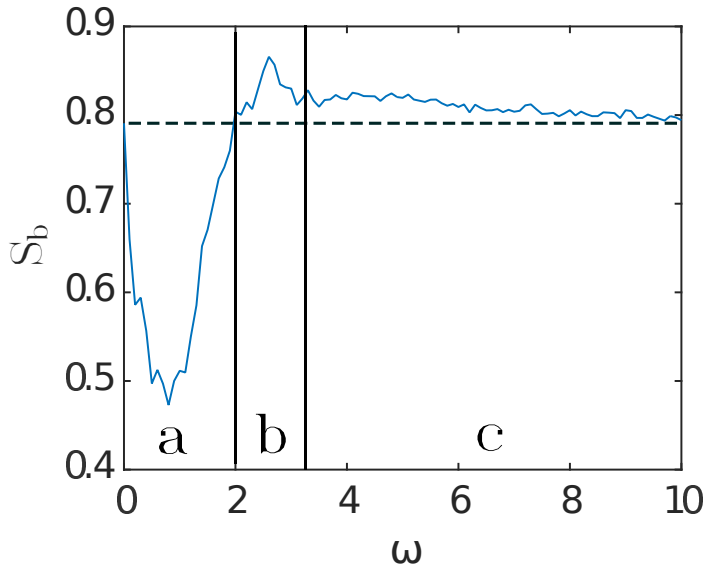


FIG. 12: (Color online) Evolution of the basin entropy with the frequency of the periodic forcing for $E = 0.19$ and $A = 0.05$. The dashed line represents the value of basin entropy of the undisturbed case. Three different regions are represented: (a) $\omega \in (0, 2.0)$, (b) $\omega \in (2.0, 3.2)$ and (c) $\omega \in (3.2, 10.0)$. It can be seen the resonant-like behavior at $\omega \approx 1$ and a maximum in the basin entropy for $\omega \approx 2.5$.

VI. CONCLUSIONS

In summary, our investigations in forced chaotic scattering reveal a resonant-like behavior in the fractal dimension of the scattering function and also in the uncertainty of the exit basins, which

has been measured using the the uncertainty algorithm and the basin entropy, respectively. In line with previous works, the main resonant frequency obtained is $\omega \approx 1.0$, for which both magnitudes are drastically reduced. As the forcing frequency increases, moving away from resonance, the forcing becomes irrelevant and the fractal dimension and the basin entropy return to their value associated with the conservative case. The resonant-like behavior appears for any nonzero amplitude and for any energy value within the nonhyperbolic regime. The decrease in the basin entropy near the main resonant frequency is due, among other things, to the reduction of the area occupied by the KAM islands and the basin boundaries. We have provided theoretical reasoning that could justify the resonant-like behavior in the fractal dimension. These arguments, based on Cantor-like structures, relate the changes in the decay rate of the exponential decay law with the fractal dimension.

We have explored the changes in the basin topology and in the escape dynamics in the resonance. We have found the amplitude value, A_c , that allows the complete destruction of the KAM islands, which is approximately constant within the nonhyperbolic regime. The same happens with the decay rate of the exponential decay law.

A context of physical interest where our work can potentially be useful is in research fields related to laser-driven reactions, chaotic Hamiltonian pumps and oscillations in chemical reactions [41–45], among others. In the context of celestial mechanics, in which the Hénon-Heiles system arises, periodic forcing could be used for modeling the effect of companion galaxies [30], such as the Magellanic Clouds orbiting the Milky Way galaxy.

ACKNOWLEDGMENTS

This work has been supported by the Spanish Ministry of Economy and Competitiveness and by the Spanish State Research Agency (AEI) and the European Regional Development Fund (FEDER) under Project No. FIS2016-76883-P. M.A.F.S. acknowledges the jointly sponsored financial support by the Fulbright Program and the Spanish Ministry of Education (Program No. FMECD-ST-2016).

[1] J. M. Seoane and M. A. F. Sanjuán, Rep. Prog. Phys **76**, 016001 (2012).

- [2] Y.-C. Lai and T. Tél, *Transient Chaos: Complex Dynamics on Finite-Time Scales* (Springer, New York, NY, 2010).
- [3] T. Tél and M. Gruiz, *Chaotic Dynamics: An Introduction Based on Classical Mechanics* (Cambridge University Press, New York, NY, 2006).
- [4] P. Gaspard, *Chaos, Scattering and Statistical Mechanics* (Cambridge University Press, Cambridge, England, 1998).
- [5] H.-J. Stöckmann, *Quantum Chaos: An Introduction* (Cambridge University Press, Cambridge, England, 1999).
- [6] H. D. Gräf, H. L. Harney, H. Lengers, C. H. Lewenkopf, C. Rangacharyulu, A. Richter, P. Schardt, and H. A. Weidenmüller, *Phys. Rev. Lett.* **68**, 2867 (1992).
- [7] G. Contopoulos and D. Kaufmann, *Astron. Astrophys.* **253**, 379 (1992).
- [8] G. Contopoulos, H. E. Kandrup, and D. Kaufmann, *Physica D* **64**, 310 (1993).
- [9] E. E. Zotos, *Nonlinear Dyn.* **89**, 135 (2017).
- [10] H. E. Kandrup, C. Siopis, G. Contopoulos, and R. Dvorak, *Chaos* **9**, 381 (1999).
- [11] J. Aguirre, J. C. Vallejo, and M. A. F. Sanjuán, *Phys. Rev. E* **64**, 066208 (2001).
- [12] R. Barrio, F. Blesa, and S. Serrano, *Europhys. Lett.* **82**, 10003 (2008).
- [13] R. Barrio, F. Blesa, and S. Serrano, *New J. Phys.* **11**, 053004 (2009).
- [14] J. C. Vallejo, J. Aguirre, and M. A. F. Sanjuán, *Phys. Lett. A* **311**, 26 (2003).
- [15] E. E. Zotos, *Meccanica* **52**, 2615 (2017).
- [16] J. D. Bernal, J. M. Seoane, and M. A. F. Sanjuán, *Phys. Rev. E* **88**, 032914 (2013).
- [17] F. Blesa, J. M. Seoane, R. Barrio, and M. A. F. Sanjuán, *Int. J. Bifurcat. Chaos* **22**, 1230010 (2012).
- [18] J. M. Seoane, J. Aguirre, M. A. F. Sanjuán, and Y.-C. Lai, *Chaos* **16**, 023101 (2006).
- [19] J. M. Seoane, M. A. F. Sanjuán, and Y.-C. Lai, *Phys. Rev. E* **76**, 016208 (2007).
- [20] J. M. Seoane and M. A. F. Sanjuán, *Phys. Lett. A* **372**, 110 (2008).
- [21] J. M. Seoane, L. Huang, M. A. F. Sanjuán, and Y.-C. Lai, *Phys. Rev. E* **79**, 047202 (2009).
- [22] J. M. Seoane and M. A. F. Sanjuán, *Int. J. Bifurcat. Chaos* **20**, 2783 (2010).
- [23] J. D. Bernal, J. M. Seoane, and M. A. F. Sanjuán, *Phys. Rev. E* **95**, 032205 (2017).
- [24] J. D. Bernal, J. M. Seoane, and M. A. F. Sanjuán, *Phys. Rev. E* **97**, 042214 (2018).
- [25] H. E. Nusse and J. A. Yorke, *Science* **271**, 1376 (1996).
- [26] E. Ott, *Rev. Mod. Phys.* **53**, 655 (1981).
- [27] G. Contopoulos, *Order and Chaos in Dynamical Astronomy* (Springer, Berlin, 2002).

- [28] M. Hénon and C. Heiles, *Astron. J.* **69**, 73 (1964).
- [29] F. Blesa, J. M. Seoane, R. Barrio, and M. A. F. Sanjuán, *Phys. Rev. E* **89**, 042909 (2014).
- [30] H. E. Kandrup and S. J. Novotny, *Cel. Mech. Dyn. Astr.* **88**, 1 (2004).
- [31] G. Contopoulos, *Astron. Astrophys.* **231**, 41 (1990).
- [32] E. Ott, *Chaos in Dynamical Systems* (Cambridge University Press, New York, NY, 1993).
- [33] J. Aguirre, R. L. Viana, and M. A. F. Sanjuán, *Rev. Mod. Phys.* **81**, 333 (2009).
- [34] Y.-T. Lau, J. M. Finn, and E. Ott, *Phys. Rev. Lett.* **66**, 978 (1991).
- [35] C. Grebogi, S. W. McDonald, E. Ott, and J. A. Yorke, *Phys. Lett. A* **99**, 415 (1983).
- [36] S. W. McDonald, C. Grebogi, E. Ott, and J. A. Yorke, *Physica D* **17**, 125 (1985).
- [37] R. L. Adler, A. G. Konheim, and M. H. McAndrew, *Trans. Amer. Math. Soc.* **114**, 309-319 (1965).
- [38] B. R. Hunt and E. Ott, *Chaos* **25**, 97618 (2015).
- [39] Y. G. Sinai, *Dokl. Phys.* **124**, 768-771 (1959).
- [40] A. Daza, A. Wagemakers, B. Georgeot, D. Guéry-Odelin, and M. A. F. Sanjuán, *Sci. Rep.* **5**, 16579 (2016).
- [41] S. Kawai, A. D. Bandrauk, C. Jaffé, T. Bartsch, J. Palacián, and T. Uzer, *J. Chem. Phys.* **126**, 164306 (2007).
- [42] D. Hennig, L. Schimansky-Geier, and P. Hänggi, *Eur. Phys. J. B* **62**, 493 (2008).
- [43] R. Ramaswamy, P. Siders, and R. A. Marcus, *J. Chem. Phys.* **74**, 4418 (1981).
- [44] T. Dittrich, M. Gutiérrez, and G. Sinuco, *Physica A* **327**, 145 (2003).
- [45] Q. Zhang, P. Hänggi, and J. Gong, *New. J. Phys.* **10**, 073008 (2008).